We are IntechOpen,
the world's leading publisher of
Open Access books
Built by scientists, for scientists

6,900
Open access books available

185,000
International authors and editors

200M
Downloads

154
Countries delivered to

Our authors are among the

TOP 1%
most cited scientists

12.2%
Contributors from top 500 universities

CLARIVATE ANALYTICS
BOOK CITATION INDEX
INDEXED

WEB OF SCIENCE™

Selection of our books indexed in the Book Citation Index
in Web of Science™ Core Collection (BKCI)

Interested in publishing with us?
Contact book.department@intechopen.com

Numbers displayed above are based on latest data collected.
For more information visit www.intechopen.com

1

High-Resolution Ion Implantation from keV to MeV

Sébastien Pezzagna and Jan Meijer
RUBION, Ruhr-Universität Bochum
Germany

1. Introduction

With the trend in miniaturisation of electronic, optoelectronic or photonic devices, it becomes necessary to control, at the highest level, the number and positioning of dopant atoms which are introduced in the devices by ion implantation. As well, new promising fields of research like quantum information processing in the solid-state also require an exact placement of implanted atoms which could be operated as the quantum bits of a future quantum computer (Ladd, 2010). In these purposes, an ideal ion implantation setup would provide deterministic single ions and nanometer spatial resolution.

In this chapter we will mainly focus on the resolution of ion implantation in the keV to MeV energy range. We will review the different ion implantation setups available at Bochum university and show the precision at which ions can be implanted along the whole energy range, that is from surface to bulk implant. Particular attention will be given to the "nanoimplanter" system with which a lateral resolution of 15 nm has been demonstrated. The nanoimplanter combines a low energy (5 kV) ion beam with the tip of an atomic force microscope (AFM) in which a nano-hole is drilled and used as a movable mask. Furthermore, a technique able to deterministically implant single ions will be presented. A section will also be dedicated to our work oriented towards the creation of defect centres in diamond which can find applications for many purposes: quantum computing, single photon sources, magnetometry, bio-labelling, drug delivery or sub-diffraction optical imaging. This latter application is directly beneficial for the ion implantation community: single defects related to nitrogen in diamond and produced by ion implantation can be imaged with a resolution of 6 nm. Sub-diffraction optical imaging offers a unique way to visualize single implanted ions at a precision approaching the one of the lattice parameter. We will use this technique along the chapter in order to precisely determine the resolution which can be achieved by the different ion implantation techniques. We have therefore implanted nitrogen ions in diamond with each of these techniques at the highest focus possible and used optical nanoscopy to directly image the implantation spots. Although we present here results obtained with nitrogen, the ion accelerators are versatile and the implantation can be extended to any kind of ions at the same resolution.

2. Spatial resolution of ion implantation and its limiting factors

In the process of ion implantation, the spatial resolution is defined as the precision in the final position of an implanted ion in the target material. It can be seen as a volume

distribution in which the implanted ions will end up. To some extend, in the case of a single ion, the spatial resolution can be assimilated as a position uncertainty around a most probable position. In this chapter, we will discuss mainly the lateral resolution. The depth resolution (implantation depth and its uncertainty) is directly related to the kinetic energy of the ion and it will be considered to have only intrinsic physical limitations. We assume that for all the implantation techniques presented here, the ion kinetic energy E is well known and that $\Delta E/E$ is negligeable.

The lateral resolution is also intrinsically-limited due to ion-matter interactions. However, the technical limitations related to the focusing capabilities of the implantation setup are in most cases predominant. In this section, the intrinsic limitations will be first briefly reviewed while the techniques to obtain the best focus will be presented in detail and discussed in section 4.

2.1 Ion straggle

Whatever the focusing capabilities of an ion implantation setup, ion straggle represents a physical intrinsic limit of the spatial resolution which can be achieved. For a kinetic ion propagating into a target material, straggling occurs due to the multiple collisions that the ion experiences at the atoms of the material. It results in a broadening of the implantation volume and can be associated to an uncertainty in the final position of each single implanted ion. The straggle is defined as the square-root of the variance of the ion distribution. It is a complex process which depends on several parameters such as the ion kinetic energy, the nature of the target material, the temperature, the crystal orientation, etc.
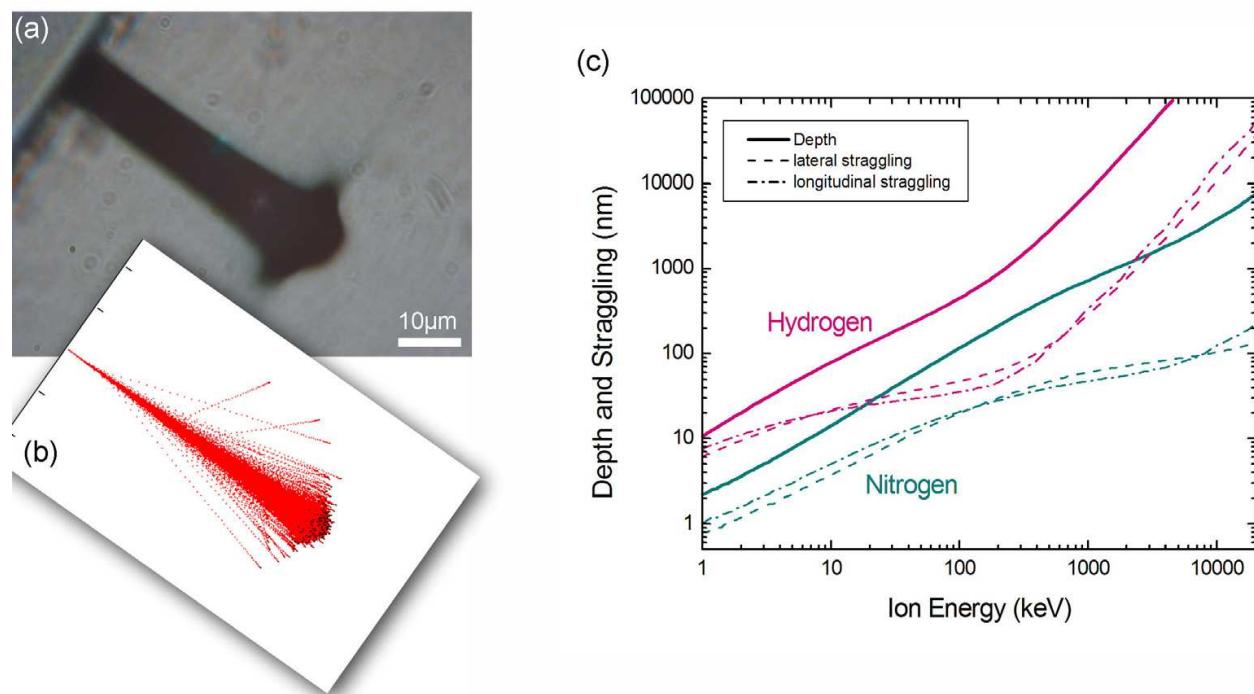

Fig. 1. (a) Optical image (side view) of a diamond sample implanted with a 3 MeV focused proton beam at high fluence. (b) SRIM simulation of 3 MeV protons implanted in diamond. (c) Plot of the ion range and straggle (lateral and longitudinal) simulated with SRIM for hydrogen and nitrogen implanted into diamond.

Figure 1a is an experimental illustration of ion straggle. It shows the side-view of a diamond implanted at high fluence with 3 MeV protons. Defects are created along the whole ion trajectory, mainly vacancies and interstitials. Above a certain ion fluence, the diamond structure gets amorphised, allowing to "see" the implantation-induced defect region. At this energy, most of the protons stop at the average depth of 49 μm, where a lateral broadening associated to straggle can be observed. In this experiment, the ion beam size is about 8 μm and the lateral resolution of the implantation is broadened up to around 10 μm due to straggle. This experiment can be simulated using SRIM (Ziegler, 2008) as shown in figure 1b. The obtained ion range is 48 μm with a lateral straggle of 1.3 μm. Figure 1c is a plot of ion range (depth) and straggle as a function of ion energy in the case of nitrogen or hydrogen ions implanted in diamond, simulated with SRIM. This graph shows that for applications requiring very high precision in the implantation of impurity atoms and aiming at nanometer resolution, a low ion energy has to be used in order to ensure a low ion straggle.

2.2 Ion channeling

Ion channeling is another effect which may be important while implanting ions into crystal substrates. Ions propagating along low-index crystallographic axes and planes penetrate deeper and produce less defects. Channeling leads therefore to a loss of the resolution in the depth direction. For a given crystal axis of the target material, channeling occurs within an acceptance angle around this axis depending on several parameters including ion nature, ion energy and sample temperature (Hobler, 1996). The part of the implanted ions undergoing channeling is hardly predictable. An experimental characterisation of channeling in the case of nitrogen ions implanted in diamond has been shown recently using secondary ion mass spectrometry (Toyli, 2010). The measured depth profiles show that a small part of the implanted ions can penetrate twice deeper as the main implantation depth.

In order to avoid channeling during implantation, the sample has to be tilted away from any channeling direction. In the case of a substrate cut along one of the principal crystallographic planes, an angle of 7° with respect to the ion beam is generally the best compromise. This is used in semiconductor technology with cubic semiconductors like silicon and germanium.

2.3 Other factors

Due to the damage induced by ion implantation, the samples generally need to be annealed in order to restore the crystal lattice. The heating process may lead to diffusion of the implanted species and therefore a broadening of the implanted volume and a loss in the resolution. In the case of diamond, the diffusion of impurity atoms is extremely small (Craven, 2009; Harte, 2009) and, under the annealing conditions that we use (2 hours at 800°C), the implanted nitrogen atoms do not diffuse to a measurable extent. This is an important point since the determination of the ion implantation resolution will be measured in diamond samples that are annealed after being implantated.

In the case of insulating samples, the surface can charge up during ion implantation. This phenomenum may be important especially in the case of low energy ions which can be electrostatically deviated from their initial trajectory. This possible loss of resolution can be

avoided by depositing a thin conductive layer on the sample before implantation or by exposing the sample to an electron shower.

3. Optical nanoscopy to measure the spatial resolution

In this section, we describe the optical methods that have been chosen to characterise the resolution of the different ion implantation techniques. We introduce the test "object" of the whole chapter, the nitrogen-vacancy (NV) centre in diamond, a very common defect in natural diamonds, responsible for pinkish colouration. Nowadays, synthetic diamonds with extremely low impurity levels can be grown by chemical vapour deposition (CVD). The concentration of nitrogen and boron (the most common impurity atoms in diamond) can be reduced to a few parts per billion. The availability of such pure substrates enables therefore an unambiguous optical characterisation of artificially-created defects.

Recently, new optical imaging techniques have broken the diffraction limit. Especially, high resolution imaging has been demonstrated using NV centres as point objects to be imaged. One of these techniques called stimulated emission depletion (STED) microscopy will be introduced in this section (Hell, 1994). Using this method, NV centres have been revealed with a lateral resolution of ~ 6 nm (Rittweger, 2009). We propose therefore to use STED microscopy in order to characterise the focusing capabilities of our ion implantation techniques. Indeed, NV centres can be easily and reliably fabricated in diamond by implantation of nitrogen followed by annealing. Typically, annealing 2 hours at 800°C in vacuum allows to restore the crystal lattice and to form the N-V bonding by diffusion of vacancies to the nitrogen atoms.

3.1 Imaging single defects in diamond

Far-field optical microscopy using focused light is an efficient way to spatially map optical centres in diamond. There are hundreds of optical centres known in diamond. Amongst these defect centres, our interest for imaging the focus of ion beams goes to the nitrogen-vacancy centre, for several reasons. The NV centre has strong optical absorption and emission, single centres can therefore be imaged using standard confocal microscopy (Gruber, 1997), it can be easily fabricated, it has a high temperature stability (up to 1500°C) and does not bleach under laser excitation. Figure 2a shows the structure of an NV centre. It consists of a substitutional nitrogen and a carbon vacancy at an adjacent lattice site. It can exist in different charge states. A room-temperature photoluminescence spectrum of a diamond containing NV centres is shown in figure 2b. This spectrum shows the zero phonon line of the negatively charged NV$^-$ centre at 637 nm and a broad vibronic band up to 800 nm. The zero phonon line of the neutral NV^0 is also visible at 575 nm. The inset in figure 2b depicts the energy diagram of the negatively charged NV$^-$.

To image NV centres in diamond we use a homemade confocal microscope. An excitation laser beam is focused on the sample through a microscope objective down to an effective confocal volume of almost 1 μm^3. The fluorescence light emitted from the excited volume is collected by the same objective and sent to the detection part of the microscope passing through a dichroic mirror (reflecting the excitation wavelength). The fluorescence is detected using an avalanche photodiode after passing through a confocal pinhole to increase

the signal-to-noise ratio. A typical saturation curve for a single NV centre (fluorescence intensity vs laser power) is plotted in figure 2d. To produce an image, the sample is scanned using a (x,y,z) piezo-element and the fluorescence is collected point after point (figure 2c). The optical resolution of a standard confocal microscope is limited by diffraction: single defects appear as a characteristic "confocal spot" of ~ 300 nm diameter. The resolution d is given by $d = \lambda / 2\,NA$ where λ is the optical wavelength and NA is the numerical aperture of the objective.
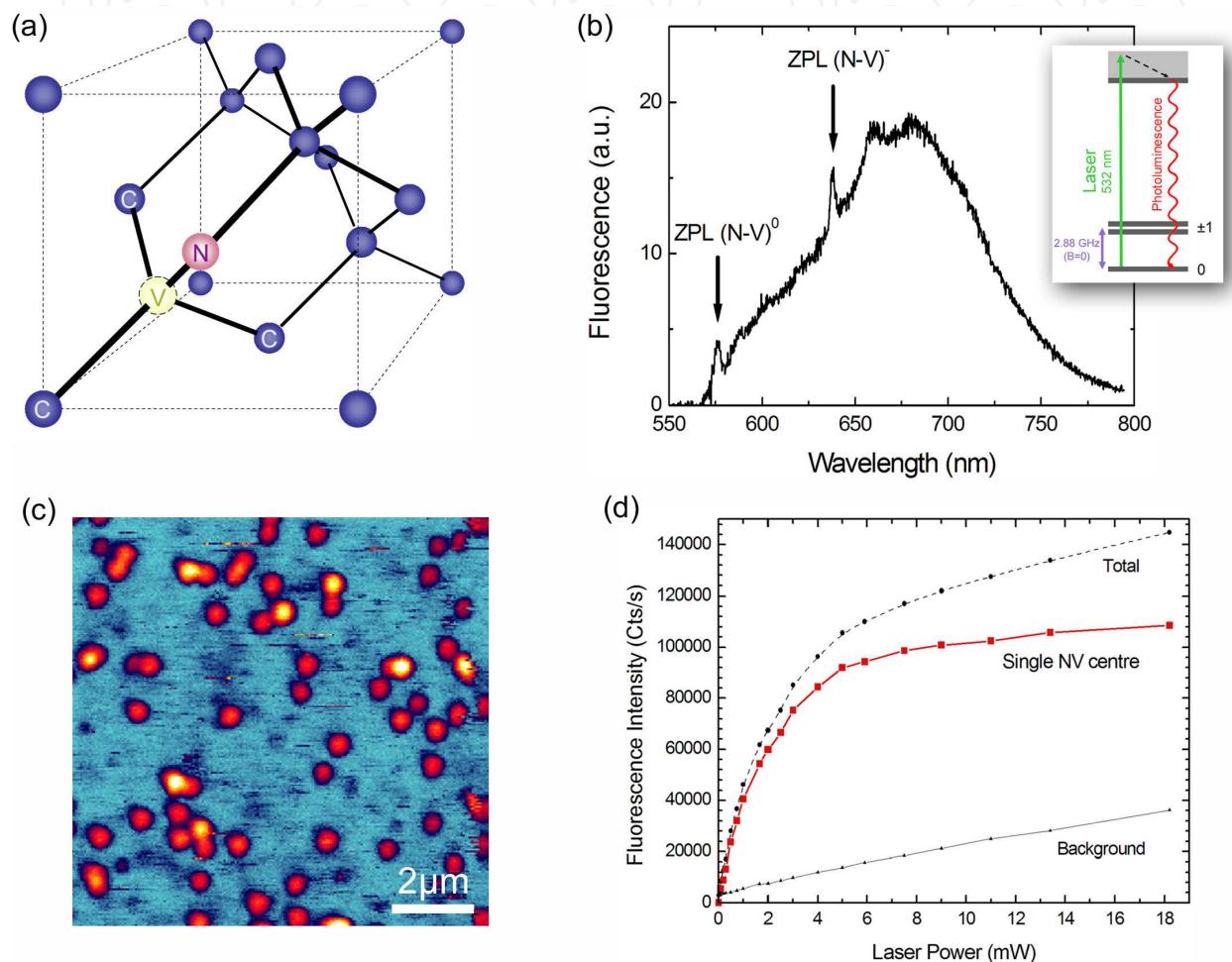
Fig. 2. (a) Structure of a nitrogen-vacancy (NV) centre in diamond, made of a substitutional nitrogen atom and a neighbouring carbon vacancy. (b) Photoluminescence spectrum of an ensemble of NV centres at room temperature with laser excitation at 532 nm (courtesy of B. Naydenov). The inset is a simplified energy level diagram of the negatively charged NV centre (Manson, 2006). (c) Confocal scan of a diamond containing single NV centres. (d) Saturation curve of the fluorescence intensity of a single NV centre as a function of the laser power.

If two or more emitting centres are separated by a distance smaller than the resolution of the microscope, they will not be optically resolved. Some of the ion implantation techniques presented in this chapter promise a beam focus in the range of tens of nanometers or even less. Confocal microscopy will therefore not provide enough optical resolution and sub-diffraction imaging techniques will be required.

3.2 High-resolution optical microscopy

A few new optical techniques have proven to break the diffraction barrier. One of these techniques is particularly adapted to image NV centres in diamond: stimulated emission depletion (STED) microscopy (Hell, 1994; Rittweger, 2009). STED microscopy is a far-field fluorescence microscopy technique which switches off fluorescent objects outside a nano-sized region using the process of stimulated emission. The simplified scheme of a STED microscope is shown in figure 3. Two superimposed laser beams are required. A green excitation beam (532 nm) having a Gaussian intensity distribution and a second beam (775 nm) having a torus intensity profile with a zero in the centre. The second beam is used in order to deplete by stimulated emission the excited level of the fluorescent objects excited by the first beam. Since the depletion beam has a zero of intensity in the centre, depletion occurs outside the centre, above a certain intensity threshold. A fluorescent object at the very centre is therefore not affected by the STED beam and shows normal fluorescence. The resolution d of a STED microscope scales with the square root of the intensity I of the depletion beam and is sensitive to the steepness of the intensity profile around the centre. It is described by:

$$d \approx \frac{\lambda}{2NA\sqrt{1 + I/I_S}}$$

where λ is the optical wavelength, NA is the numerical aperture of the objective, and I_S is the characteristic saturation intensity of the NV centres. The setup that has been used for the measurements presented in this chapter is equipped with pulsed excitation and depletion beams (~ 100 ps pulse duration).
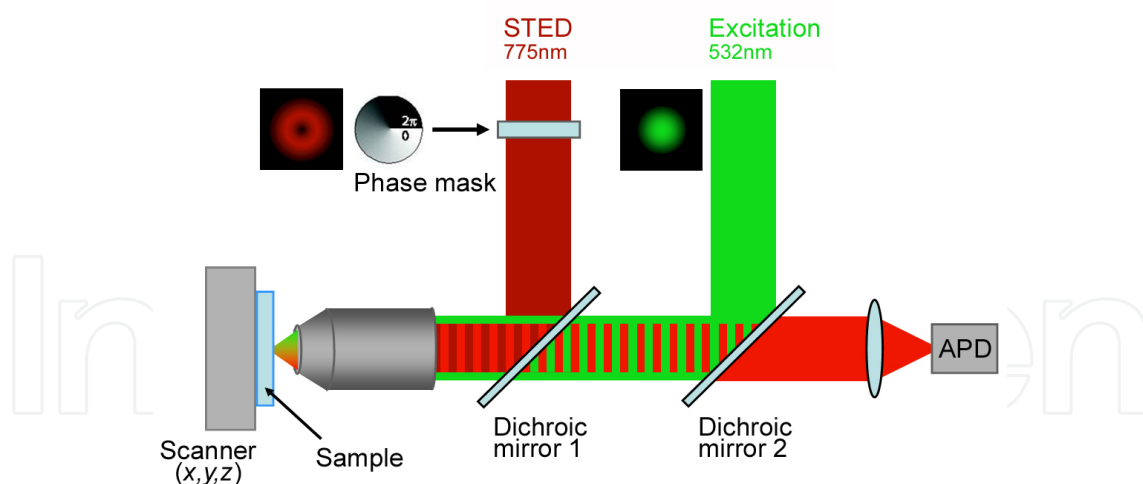

Fig. 3. Simplified scheme of the stimulated emission depletion (STED) microscope used at the Max Planck Institute in Göttingen, Germany (group of S. W. Hell).

They are synchronized to arrive simultaneously on the sample. The fluorescence signal incoming from the reduced nano-sized area is collected after application of the pulses. The images are obtained by scanning the sample mounted on a piezo-stage.

STED microscopy is possible with NV centres because they possess a strong electron-phonon coupling and therefore a large PL sideband (excitation and depletion beam can be

spectrally well separated). Moreover, their high photo-stability allows to apply high laser intensities for the depletion beam and therefore to reach high resolutions.
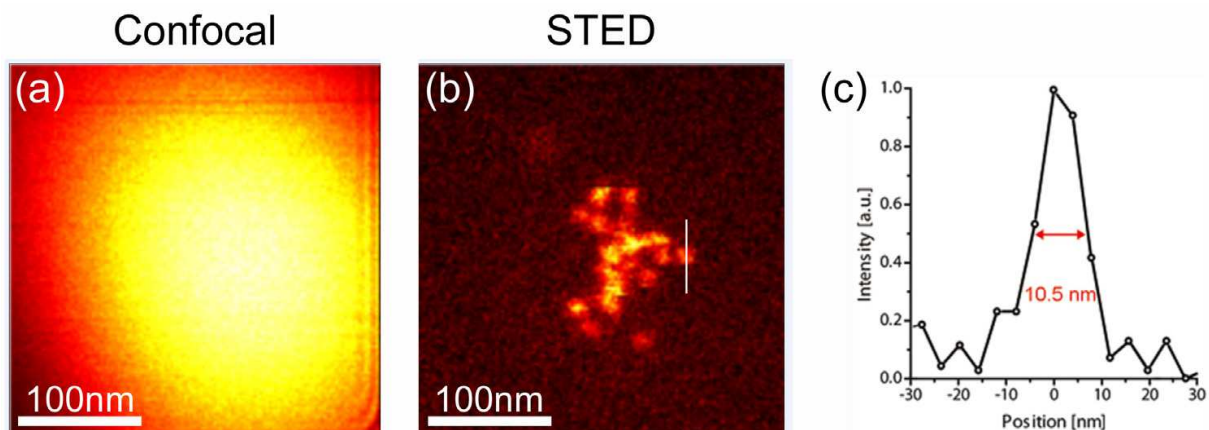

Fig. 4. Optical imaging by far field microscopy of NV centres created in diamond by implantation of 5 keV nitrogen ions through a 120 nm aperture (Pezzagna, 2010b). Optical measurements have been done at the MPI Göttingen, Germany (group of S. W. Hell). Both images are 300x300 nm² scans of the diamond surface. (a) Confocal imaging is diffraction-limited to ~ 300 nm. (b) STED breaks the diffraction limit and allows to visualise each optical centre individually. (c) Intensity profile (line in (b)) of a single NV centre imaged by STED microscopy.

An example of the imaging capabilities of STED microscopy in comparison with confocal microscopy can be seen in figure 4. In this purpose, NV centres have been created in diamond by implantation of nitrogen (5 keV, fluence 3×10^{13} cm^{-2}) through a nano-aperture of diameter ~ 120 nm. Figure 4a shows the confocal fluorescence image of the diamond surface where the nitrogen ions have been implanted. From the observed bright spot it is impossible to retrieve the size of the aperture through which the NV centres have been created. The number of NV centres present within the spot may be estimated by integrating the intensity and comparing it to the intensity of a single NV centre. Note that for a small number of NV centres, the study of the photon statistics using a "Hanbury Brown Twiss interferometer" can also give access to the number of emitting centres (Jelezko, 2006). However, in both cases, no spatial information can be found. In contrast, the STED microscopy image is shown in figure 4b. Due to the strong increase in optical resolution, almost all NV centres can be imaged separately. This allows to determine precisely the size of the aperture used during the ion implantation. Note that implanting a higher nitrogen ion fluence and therefore obtaining a higher density of NV centre would give an even better image of the 120 nm aperture. Figure 4c shows the intensity profile of a single NV centre corresponding to the line in figure 4b. The optical resolution of the STED microscope is here about 10 nm.

4. Ion implantation setups from keV to MeV

In this section, the different ion implantation techniques that are in use at the university of Bochum are presented. They cover a wide ion energy range from keV to MeV and therefore implantation depths from the very first nanometers to several micrometers or tens of

micrometers. For each of these techniques we will show and discuss their capabilities in terms of resolution.

4.1 4 MV Tandem accelerator

Different types of accelerators provide ions with high kinetic energy. Ion implantations with kinetic energies from a few keV up to a few MeV can be produced by electrostatic accelerators. The main parts of an accelerator are the ion source, the generator which provides the acceleration voltage and the mass analyzing magnet. The setup of the ion source depends on the desired ion species and the requested ion current. There are a large number of sources available. The generation of the high voltage can be provided electrically (e.g. using a Crockoff-Walton circuit) or by mechanical charge transport as realized in a van de Graff or in a Pelletron accelerator. In the MeV regime, the electrical solutions provide a higher stability but are of higher complexity. The mass separation is easily achieved by magnetic fields. For low energy beams it is possible to install the mass separation before the acceleration takes place in order to reduce the necessary field strength. Beside these compounds, ion focusing and steering systems are necessary. The properties of an accelerator are defined by its energy resolution, beam size and current for a given ion species. The energy resolution $\Delta E/E$ depends on the stability of the ion source and the high voltage generation. Using modern electronics, $\Delta E/E < 10^5$ are typically available.

The 4 MV Dynamitron Tandem accelerator available at the university of Bochum can provide ions in the energy range 300 keV to around 50 MeV, depending on the ion charge state. Ion currents up to 100 μA can be reached. Elements are available as kinetic ions provided they can be negatively charged. This accelerator is suitable for deep implantation of ions in so-called bulk conditions, generally far from the surface influence. For the implantation of large structures in a short time, the system is equipped with an ion projection setup (not presented here). For the implantation of fine structures or of single ions we use two different techniques: either directly focusing the beam to the sample using a strong magnetic field or implanting through a mica mask containing nano-channels with high aspect ratio.

4.1.1 Focusing with single lens superconductive solenoid

Microbeam systems are under development since the seventies. Most systems are based on quadrupole lenses to focus MeV proton beams for analytical purposes. For a maskless ion implantation, the focusing of heavy ion beams is necessary. Additionally, a fast change of the focusing power is useful. Electrostatic lenses are too weak for this purpose and only magnetic fields meet all the requirements.

A maskless and focused ion implantation below 1 μm can be achieved using a single-lens system based on a superconductive 14 T solenoid without any ferromagnetic core. Such a system has been developed in Bochum. A focusing power of 100 MeV a.m.u. can be achieved which is enough to focus any ion in the energy range from 500 keV to more than 20 MeV. Moreover, a fast and easy change of ion species and/or ion energy can be done within 30 minutes. The chromatic aberration is comparable to the one of quadrupole systems. However, the spherical aberration is about one order of magnitude smaller. The smallest spot size achieved is about 400 nm, which corresponds to the expected theoretical value (as

considering the diaphragm size and demagnification factor). However the alignment and the focusing are extremely sensitive and the beam focus can hardly be reduced below 1 μm. An electrostatic octupole placed inside the lens is used in order to scan the beam and to correct the lens aberrations. A scheme of the system can be seen in figure 5a. A standard beam focus can be estimated from figure 5b. It shows an array of spots made of a few NV centres which has been created by the focused implantation of ~ 30 nitrogen ions (energy 11 MeV) per spot. In these conditions, the NV centres are 4.2 μm deep and the expected ion straggle is about 120 nm. It can be seen that the beam focus is in the range of 1-2 μm. Better focuses have nevertheless been achieved for the creation of pairs of close-by NV centres (Meijer, 2005; Neumann, 2010) or of intrinsic TR12 centres (Naydenov, 2009).
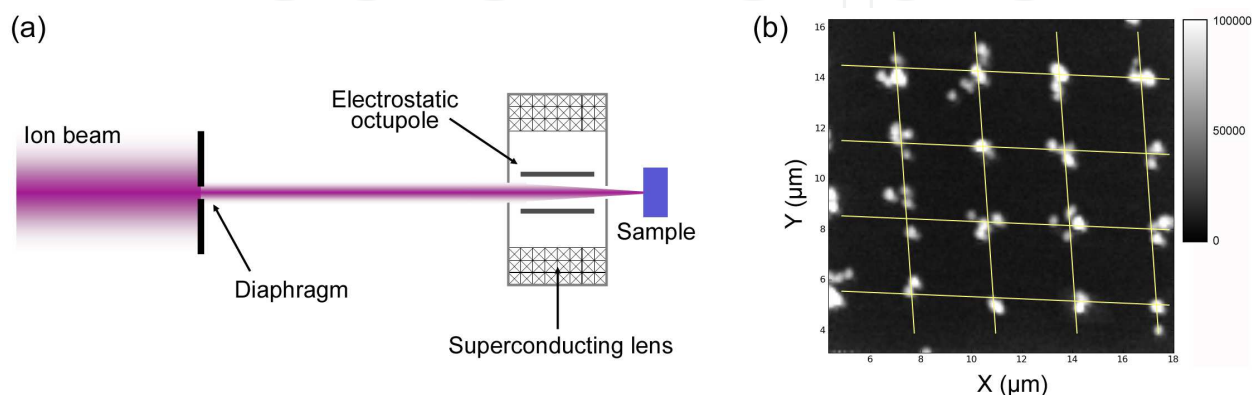

Fig. 5. (a) Scheme of the ion microbeam setup. The ion beam delivered by the accelerator is formed by an aperture and focused with the superconductive solenoid lens on the target. An in-lens electrostatic octupole is used for correction of the lens aberration and for scanning the ion beam (Pezzagna, 2011a). (b) Confocal fluorescence microscopy scan of an ultrapure diamond implanted with 11 MeV nitrogen ions. The focused beam has been scanned in order to produce a pattern of NV centres with a distance of 3 μm. The average number of implanted N per spot is 30. Each bright spot corresponds to a single NV centre.

4.1.2 Collimating through nano-channels in mica

Another possibility to obtain high-resolution implantation using MeV ions is to use a mask. However, fabricating a mask able to collimate an MeV ion beam to a few tens of nanometers is not trivial. It requires small channels inside a thick material to stop energetic ions, and therefore with a high aspect ratio. In what follows, we show how mica can be used in such a way, how nano-channels with an aspect ratio higher than 100 can be fabricated and how ions can succesfully be implanted through the nano-channels. The nano-channels are fabricated in a two step process. First, mica (muscovite) layers of 5 to 30 μm thickness are irradiated by swift heavy ions, samarium with an energy of 1,6 GeV. The energy is high enough so that the ions go through the mica layer while they produce an ion track of amorphous material (a few nm in diameter) across the mica sheet. The amorphous material in the tracks presents a higher etcheability and can therefore be removed chemically in a second step (Khan, 1981). We use an aqueous solution of hydrofluoric acid at 10%. The result of such a process can be seen in figure 6a. Nano-channels with very smooth walls are formed in the mica, all having the same rhombus-shaped opening. The size of the channels depends on the time the layer is left in the acid solution. Channel sizes below 30 nm have been demonstrated in 5 μm thick mica (Pezzagna, 2011b). Figure 6b shows the result of the

implantation of nitrogen ions in diamond through such a mica layer with nano-channels. The fluorescence scan of the diamond after annealing reveals the creation of NV centres. Each bright spot corresponds to the fluorescence of one or several NV centres. We have unfortunately not yet the possibility to show high-resolution STED microscopy pictures of the single spots, however, previous measurements indicate that average spot size is approaching the limit of the ion straggle. This result shows an increase in resolution of one order of magnitude in comparison with the focusing using a superconductive lens. Regarding the high aspect ratio of the nano-channels, it is however important to characterise the transmission of ions through the mica layer. We first can indirectly estimate the transmission by measuring the average number of NV centres created by the implantation of N through a single nano-channel. We assume a creation yield of NV centres of 15% (Pezzagna, 2010a). By measuring the second order autocorrelation function of the photon emission statistics coming from each fluorescence spot (Hanbury Brown, 1956), we found out that approximately 4% of the ions have been transmitted. To verify this estimation, we performed a direct measurement of the transmission by shooting 1 MeV nitrogen ions on a mica layer with nano-channels and using an ion detector placed directly after it. The layer has been mounted on an 100 μm diameter aperture which can be tilted with respect to the ion beam. In this experiment, the rate as well as the energy of the transmitted ions have been measured as a function of the tilt angle. At maximum, the transmission is about 1% and an energy broadening of the transmitted ions of about 175 keV is observed. If the mica is slightly tilted (1.7°), the transmission strongly drops down and the energy maximum is shifted down to 650 keV with a FWHM of about 500 keV.
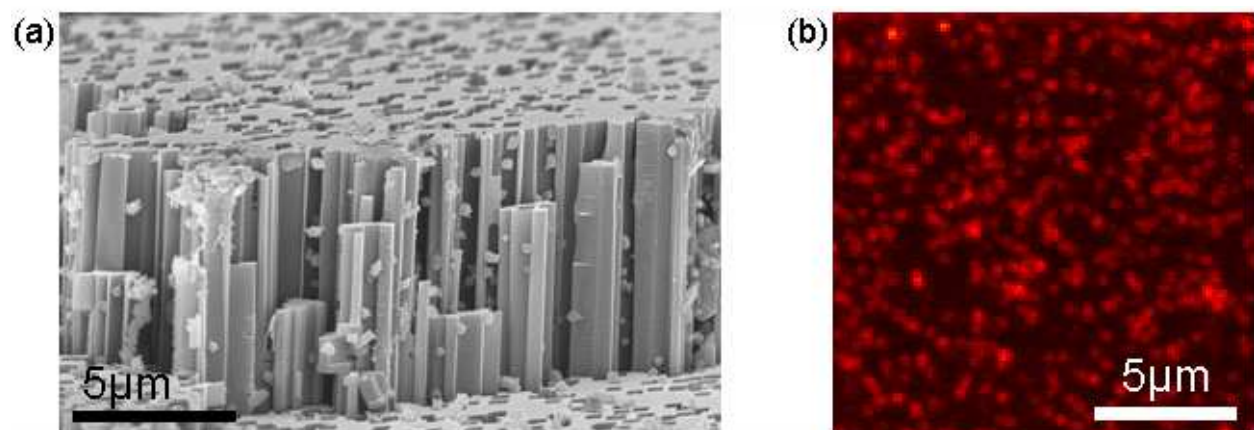

Fig. 6. (a) Mica layer with nano-channels (Pezzagna, 2011b). (b) Confocal fluorescence scan of an ultrapure synthetic diamond implanted with 1 MeV nitrogen ions through the mica layer. Each spot corresponds to one or more nitrogen related optical centres.

Details of the experiment can be found in reference (Pezzagna, 2011b). The energy broadening and the decrease of the energy maximum of the transmitted ions indicate that ions are scattered at the walls of the nano-channels where they lose energy. We attribute this to a misalignment of the ion beam and the nano-channels. Charging up of the mica layers may also contribute to limit the transmission. Further investigations have to be done in order to improve the transmission, however this technique offers an implantation resolution for MeV ions approaching the straggling limit. In the future, single nano-channels will be used to collimate high energy ion beams in order to achieve patterned implantations with high resolution.

4.2 100 kV negative ion accelerator

In the energy range of a few tens of keV or less, it is possible to use resist and electron beam lithography to achieve high-resolution ion implantation. Typically, using PMMA photoresist, one deposits a few hundreds of nm on top of the substrate. This means that the energy of the ion has to be low enough to preclude any transmission through the resist mask.
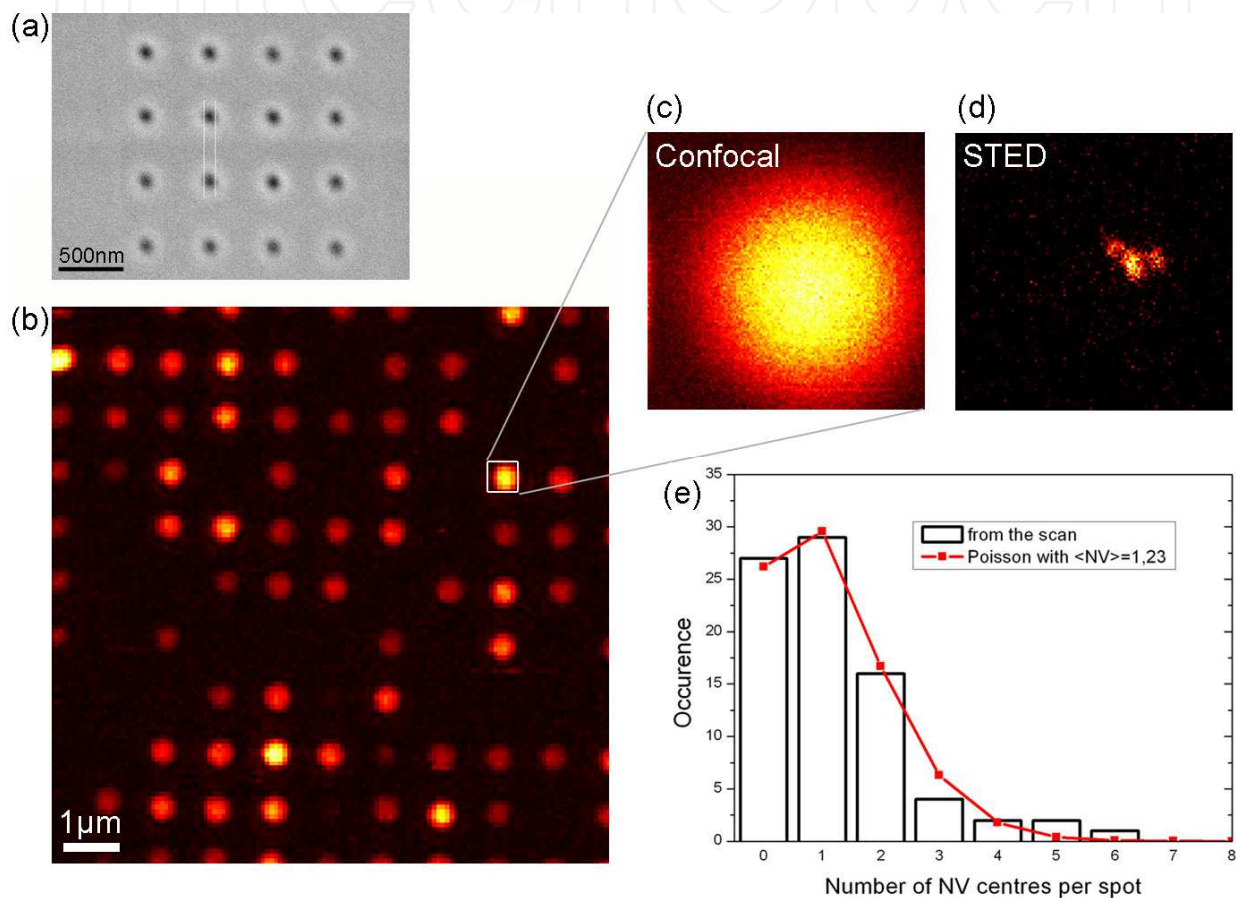

Fig. 7. (a) SEM image of a PMMA photoresist mask patterned by electron beam lithography. The estimated hole diameter is 65 nm and the resist thickness is 230 nm. (b) Confocal fluorescence image of the surface of a diamond implanted with 55 keV CN⁻ molecules through a PMMA mask. (c) Zoom on the inset in (b). (d) STED image of the same confocal spot, the single NV centres can be resolved. (e) Distribution of the number of NV centres per spot, fitted by a Poisson distribution with an average value of 1,23.

The creation of NV centres in diamond with this technique has already been demonstrated with 80 nm resolution (Spinicelli, 2011; Toyli, 2010). A compromise has to be found between the resist thickness and the smallest details that one wants to achieve into the photoresist. The use of a PMMA mask suits the 100 kV negative ion accelerator that is operated in Bochum. A SEM picture of a PMMA with ~ 65 nm holes made by e-beam lithography is

shown in figure 7a. The creation of NV centres by implantation of CN- molecules is shown in figure 7b. Here also, confocal microscopy cannot provide informations on the spatial resolution. We have therefore used STED microscopy on the brightest spot containing the highest number of NV centres (figure 7c and 7d). The dimension of the spot (although not circular) is about 60-80 nm which is in good agreement with the size of the holes observed in the PMMA layer.

Note that this accelerator enables the implantation of CN- molecules which can be a unique method to create a pair made of an NV centre and a close by ^{13}C. As it will be seen in the last section, the electron spin associated to an NV- centre can be coupled with the nuclear spin of a ^{13}C atom (provided both are separated by only a few nm) to build a quantum register operating at room temperature.

4.3 5 kV nanoimplanter

In order to aim at the highest positioning precision of implanted ions, one has to reduce the ion energy to a few keV or less. The 5 kV "nanoimplanter" is dedicated to ion implantation with the smallest straggle possible and therefore targeting nanometer resolution. It combines a low energy ion gun with an atomic force microscope (AFM), the tip of which is pierced with a nano-hole (Meijer, 2008; Pezzagna, 2010b). Focusing such a low energy (a few keV or less) ion beam to nanometer spot size is almost impossible due to chromatic aberrations. The principle of the setup is therefore to use the nano-hole in the AFM tip as a collimator of the ion beam which can moreover be addressed at any place of a substrate. This system offers the possibility for example to previously image with the AFM tip a structure in which ions have to be implanted (a photonic crystal, a planar micro-LED, a quantum dot, etc.) and then to run the implantation process. The setup built in Bochum is equipped with a gas-source ion gun (5 kV, SPECS IQE 12/38) combined with a Wien mass filter (E×B). This provides positive species of any inert gas (He, Ar, Ne, Xe, Kr, N$_2$) as well as reactive ions by use of O$_2$ or H$_2$. However, this source can be replaced by a liquid metal ion source to extend the implantation possibilities to other atoms. The ion currents can be in the range 10 µA to less than 1 pA and the acceleration voltage can be tuned from 5 kV down to 0,2 kV. A supplementary single electrostatic lens is used in order to focus the beam to the sample. The minimum beam diameter obtained at the target sample position can be reduced by using an aperture a few µm large placed before the single lens. The sample holder is mounted on the piezo-electric scanner of the AFM which allows nanometer placement in a range of 60 µm. The AFM scanner itself is mounted on a long-range step-motor table providing µm placement over several centimeters. The ion beam current is measured using a Faraday cup fabricated directly on the sample holder and using a picoamperemeter. In the case of very low currents, an electron multipler (detection efficiency > 90%) allows to detect single ions. In order to align the AFM tip to the ion beam, an in-situ microscope objective (10x) gives a live view of the sample. The AFM system (PI Instrument) works in contact mode and uses piezoresistive cantilevers (Persaud, 2006). The AFM cantilever and tip are made of silicon nitride and the tips are hollow. A view of the system is shown in figure 8a. It is mounted on a vibration-free optical table and an ion pump is used during the ion implantation with the tip in order to avoid vibrations. Figure 8b is a view inside the chamber and figure 8c is a scheme of the setup showing the Faraday cup and the electron multiplier (both not visible in figure 8b) which are used to measure the ion beam current.
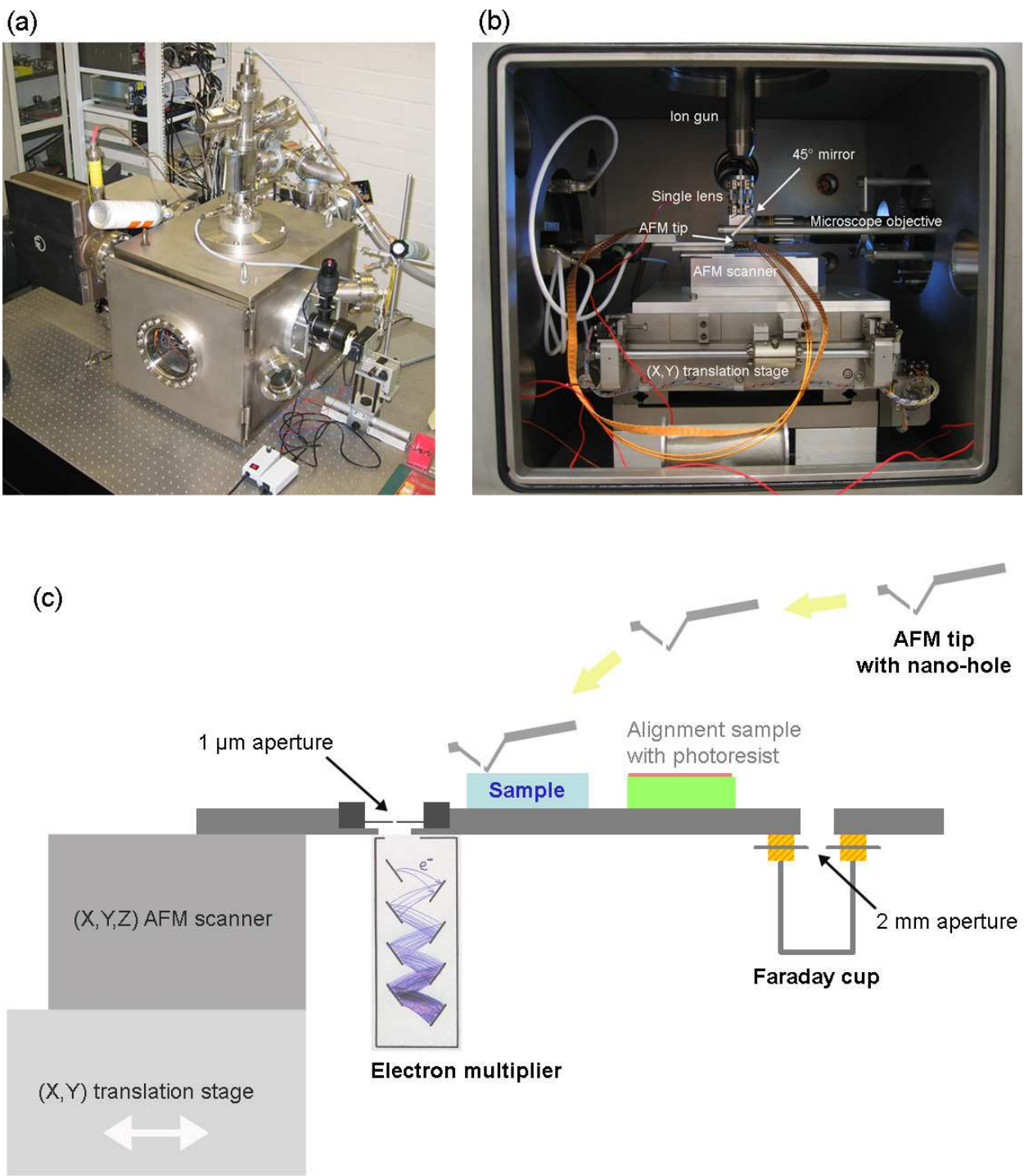
Fig. 8. 5 kV ion implanter combined with an AFM. (a) Picture of the chamber placed on a vibration isolated optical table. (b) View inside the chamber. (c) Scheme of the sample holder. The ion beam is fixed, therefore the sample holder can be moved using the combination of a long range translation stage and the scanner of the AFM. The AFM tip is controlled by another (X,Y,Z) arm.

4.3.1 Drilling the nano-hole by focused ion beam

The nano-holes used to collimate the ion beam are drilled by focused ion beam (FIB) from the backside of the AFM tip (figure 9a and 9b). A thin (a few nm) conductive layer is generally deposited before the FIB process in order to avoid any charging up of the tip which is based on silicon nitride. A Faraday cup may be placed below the AFM tip which has to be drilled so that as soon as a hole is pierced an ion current can be measured and the ion beam stopped. It is generally preferred not to drill the hole directly at the summit of the tip (figure 9c) because it may be damaged or closed when in contact with the substrate to be implanted. The hole shown in figure 9c has a diameter of about 80 nm. We choose the facet presenting the highest incidence angle with respect to the ion beam in order to increase the hole lifetime under ion bombardment. Due to the fact that the pyramidal tip is hollow and thin, the holes can be drilled in a few seconds using 30 keV Ga^+ ions and a 10 pA current. A typical example of collimated implantation through such a hole can be found in figure 4. It will be described in section 4.3.3 how the size of the holes drilled by FIB can be reduced.
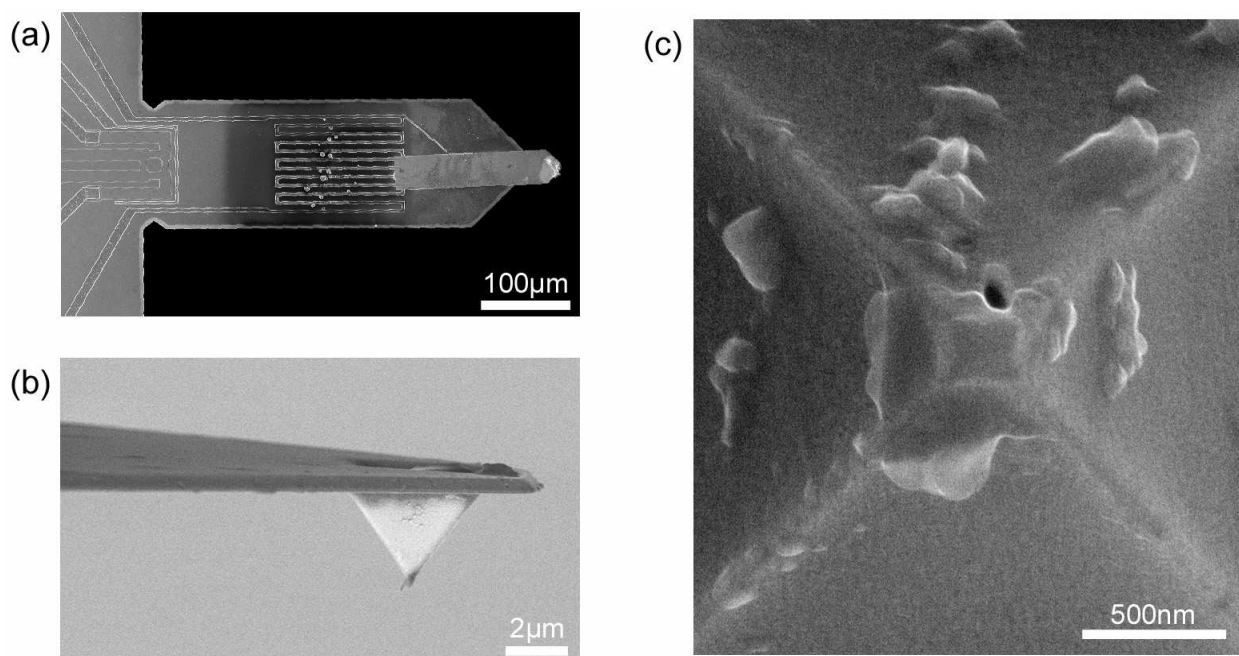

Fig. 9. (a) SEM image of the piezo-resistive cantilever at the end of which the tip is glued. (b) SEM image of the hollow pyramidal AFM tip. (c) SEM image of the summit of the tip where a nano-hole has been drilled by focused ion beam milling.

4.3.2 Alignment between AFM tip and ion beam

We use a piece of silicon covered with PMMA photoresist which is sensitive to the ion beam. The position of the ion beam, as well as its diameter (figure 10a), can be precisely measured in situ using a microscope objective (10x). The AFM tip is then aligned to the imprint of the ion beam (figure 10b) which is confirmed by the shadow of the tip eclipsing a part of the ion beam. In most of the applications, we use a large beam diameter (~ 20 µm) which allows an easy alignment.

If the hole is placed close to the edge of the tip, there will be an implanted halo around the tip. This should however be avoided for some specific applications. In such a case, one can

either use a smaller beam focus (however with a more delicate alignment step), or use another type of tip in which the hole is located in the middle of a much larger cantilever thus allowing to use large beams and still ensure excellent alignment.
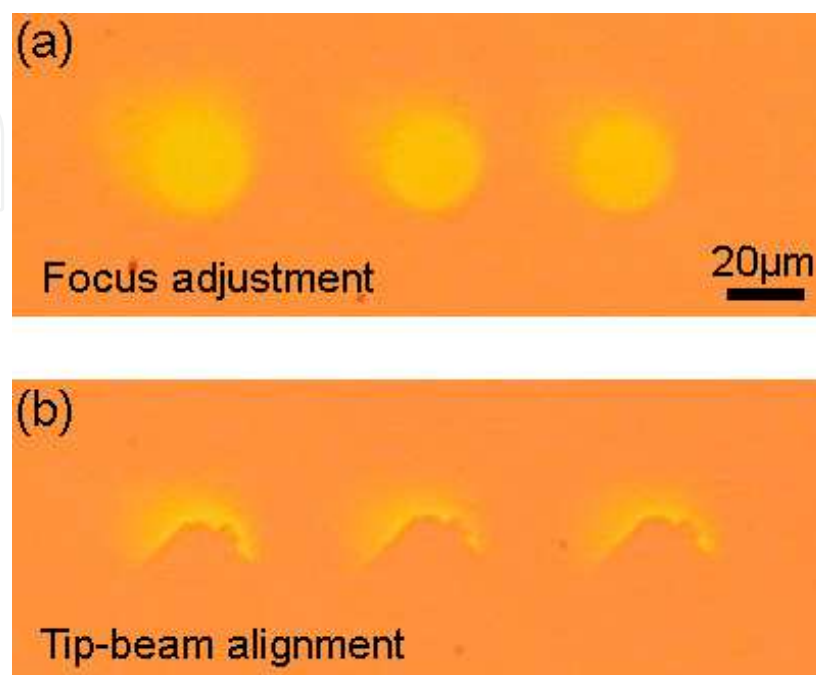

Fig. 10. In situ beam characterisation using PMMA photoresist. (a) Impact of the ion beam on PMMA at different focusing voltages of the single lens for focus adjustment. (b) Alignment of the mobile AFM tip to the fixed ion beam.

4.3.3 Reducing the size of the nano-holes

It has been shown that ion beam irradiation could lead to a reduction in the size of nano-apertures. Li (Li, 2001) named this effect ion beam sculpting. We observe the same phenomenon for the nano-holes in the AFM tips (Pezzagna, 2010b). Therefore, there exists a way to control the closing or even opening of the nano-holes in a more or less limited way. This allows to reach extremely small collimation of the ion beam and to perform ion implantion at very high spatial resolution. Figure 11a shows the creation of NV centres by implantation through a hole, the size of which has been previously reduced from 100 nm to below 20 nm by ion beam sculpting. The STED image reveals an implanted spot (FWHM of 21 nm) in which the single NV centres can no more be resolved (figure 11b). The optical resolution of the STED microscope is here of 10 nm. A critical point for this technique to ensure the collimating of the ion beam is the distance between the nano-hole and the substrate. The use of the AFM tip guaranties an excellent control of this distance. In case the hole is far away from the surface (a few μm), undesired scattered ions may broaden the implantation resolution. The technique using the pierced AFM tip provided to date the highest precision in the creation of NV centres in diamond. It is important to note that using the nano-hole as collimators, any kind of ions can be implanted and not only nitrogen.
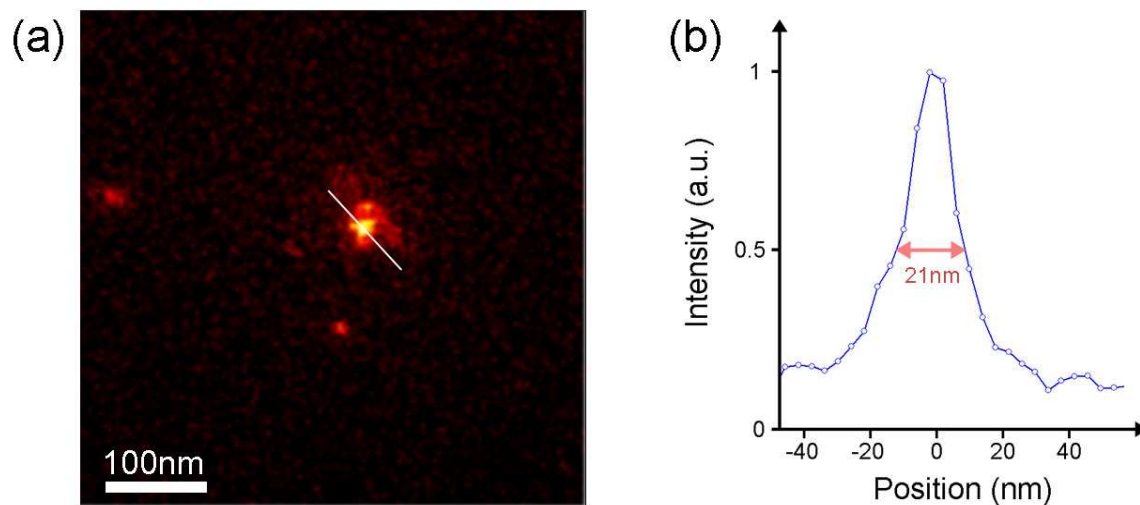
Fig. 11. (a) STED microscopy scan of the spot of NV centres created by implantation of 5 keV nitrogen ions through a reduced nano-hole. (b) Intensity profile corresponding to the line seen in (a). The optical resolution of the STED microscope is here 10 nm.

4.4 Towards deterministic ion implantation

An ideal ion implantation setup would provide nanometer spatial resolution of deterministic single ions. We have just seen that resolution below 20 nm is possible and that furthermore it can be even improved. However only a statistic number of ions can be implanted. Although single implanted ions can be detected in some specific cases where the secondary electrons produced by the impacts in the target are recorded, it would be much more advantageous to directly shoot deterministic single ions from the accelerator. In this view, the most promising method relies on an ion Paul trap out of which single ions can be extracted and further accelerated and focused. Schnitzler et al. show that deterministic single Ca^+ ions can be shot out of such a trap and detected by an electron multiplier (Schnitzler, 2009). In terms of focusing, nanometer regime can theoretically be reached provided the ions in the trap can be cooled down to their motional ground state. Energies in the keV range should be reacheable as well as extraction rates in the kHz regime.

5. Applications of optical centres in diamond

There are several hundreds of optical centres known in diamond (Zaitsev, 2001) which cover a large spectral range from ultraviolet to near infrared. The most prominent of them are the nitrogen-vacancy NV centre, the silicon-vacancy SiV centre, the nickel-related NE8 centre, or the chromium-related centres. All of these defects in diamond have been observed as single centres and have shown single photon emission under optical excitation. One of the greatest advantages of optical defects in diamond is their high stability and the possibility to create some of them artificially, especially by high-resolution ion implantation, in bulk diamonds but also in nano-diamonds. Diamond-based robust single-photon-sources using NV centres (Kurtsiefer, 2000) are nowadays finding remarkable applications in many fields of physics (applied and fundamental). They have been used for quantum cryptography (Beveratos, 2002; Alléaume, 2004) or single photon interference (Jacques, 2007). Electrically triggered single-photon-sources are however still missing.

In biology and medicine, NV centres imbedded in nanodiamonds are widely used as fluorescent labels (Faklaris, 2008; Fu, 2007). They combine the advantages of high brightness, excellent photostability and non-toxic nature of the nano-diamonds. The continuous imaging of the digestive system and the cellular development of living worms feeded with nano-diamonds has for example been demonstrated (Mohan, 2010).

Another promising application of the NV centre is quantum registers. The electron spin associated to one single NV- centre can be polarised and read out optically and manipulated using microwave pulses (Jelezko, 2004). Moreover, the coherence time of the electron spin can be as long as 2 ms (Balasubramanian, 2009) in isotopically engineered diamonds (with reduced [^{13}C] concentrations) which has no equivalent in the solid state at room temperature. The achievement of basic quantum information protocols necessitates multipartite entangled states. Several qubits have to be coupled and controlled independently in order to create such quantum states. This can be achieved in diamond at room temperature; quantum registers using the interaction between the electron spin of an NV defect and other neighbouring spins in the diamond matrix (nuclear spins of ^{13}C isotopes or of the nitrogen atom itself) have been demonstrated at 300K (Gurudev Dutt, 2007). A scalable quantum information architecture would however require the coupling between distant NV centres. In the case of ultrapure CVD diamond substrates, the distance should not exceed 20 nm (to keep coupling prevailing over decoherence). A quantum register has also been demonstrated using the dipolar magnetic coupling between the electron spins of two NV centres separated by 9 nm (Neumann, 2010). These NV centres have been produced by the focused implantation of 2 MeV nitrogen ions. To create scalable NV centres further efforts are however necessary: increase the creation yield from N to NV during annealing (Pezzagna, 2010a) and achieve deterministic implantation of single nitrogen ions.

High sensitivity magnetic sensors can also be realized using the spin properties of the NV centres (Balasubramanian, 2008; Degen, 2008; Maze, 2008). In the case that a magnetic field is applied in the vicinity of an NV centre, the ground state sublevels (m_s=±1) are splitted by the Zeeman effect. This splitting can be measured by optically-detected magnetic resonance technique. The frequency splitting between the two resonance lines is directly related to the amplitude of the magnetic field. More sophisticated and sensitive techniques are based on the determination of the magnetic field through the dephasing that it induces in Ramsey-type experiments (Taylor, 2008). Two magnetometry approaches are possible: using a single NV spin attached at a scanning probe or using ensemble of NV centres. The first approach provides high resolution imaging while the second reaches high detection sensitivity.

For future quantum communication, the NV centre is however not the ideal single-photon-source (Aharonovitch, 2011; Pezzagna, 2011a). Both in terms of spectral width and of emission rate, other defect centres have been found (especially the "Chromium-related centres") which provide higher photon rates with narrower emission bandwith. Unfortunately, it has not yet been possible to produce these centres in a reproducible way neither by ion implantation nor during diamond growth. As a result, there is still a large field to explore in the search of an ideal single-photon-source in diamond and the versatility of ion implantation makes it be the technique of choice.

6. Conclusion

Ion implantation is a unique tool which makes it possible to artificially place impurity atoms in any host substrate. New implantation techniques allow for more precisely controlling the position of implanted ions. In this chapter, we have reviewed some of the techniques providing the highest focus for ion beams on a large energy range. To give a relevant comparison, we have implanted nitrogen ions in diamond with each of these techniques in order to produce the so-called nitrogen-vacancy (NV) defect centres. An extremely precise determination of the lateral resolution was made possible by optically imaging the single NV defects produced by implantation and taking advantage of the exceptional imaging capabilities of new sub-diffraction optical microscopy. There is a physical limit to the ion implantation resolution, mainly due to straggle and channeling. For a given ion and target material, this limit depends only on the ion's kinetic energy. Therefore, the implantation resolutions obtained with techniques providing ions in different energy ranges should also be compared with the intrinsic limit at the corresponding energies.
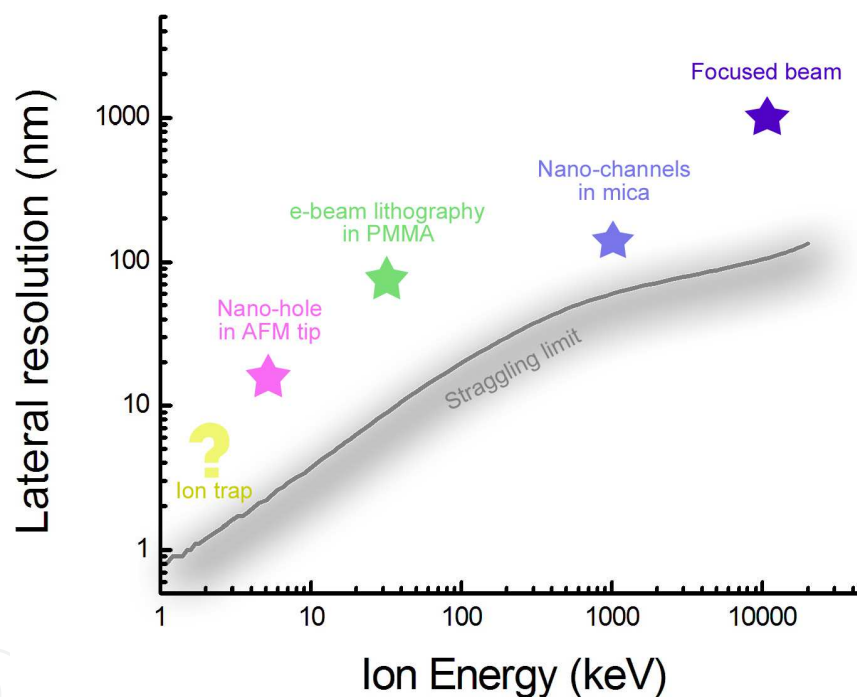

Fig. 12. Lateral resolution vs ion energy plot of the state of the art ion implantation of nitrogen in diamond. The grey line represents the lateral straggle for nitrogen in diamond.

Figure 12 is a plot of the state of the art lateral resolution which has been demonstrated at different ion energies in the case of nitrogen ions implanted in diamond. The lateral straggling is also plotted. The highest implantation precision (15 nm) has been obtained by collimating the ion beam using an AFM tip pierced with a nano-hole (Pezzagna, 2010b). It is possible to even improve this resolution as it has been shown that nano-hole diameters can be reduced using the ion sculpting technique (Li, 2001). Note that the AFM-implanter system provides ions possessing the lowest energy of all the techniques presented here and therefore the lowest ion straggle. In the case of MeV ion beams, the collimation by nano-channels in mica offers a precision approaching the straggle limit (Pezzagna, 2011b). Since

this is a very new technique, further research will be necessary, especially to improve the transmission of ions through the nano-channels.

Apart from the placement precision, the control of the number of implanted ions becomes crucial in smaller implanted devices. Promisingly, the method based on an ultracold ion trap (Schnitzler, 2009) presented in section 4.4 has already made possible the deterministic implantation of countable single ions for the first time.

7. Acknowledgment

8. References

Aharonovich, I.; Castelletto, S.; Simpson, D. A.; Su, C.-H.; Greentree, A.-D. & Prawer, S. (2011). Diamond-based single-photon emitters. *Reports on progress in Physics*, Vol. 74, pp. 076501

Alléaume, R.; Treussart, F.; Messin, G.; Dumeige, Y.; Roch, J.-F.; Beveratos, A.; Brouri-Tualle, R.; Poizat, J.-P. & Grangier, P. (2004). Experimental open-air quantum key distribution with a single-photon source. *New J. Phys.*, Vol. 6, p. 92

Balasubramanian, G.; Chan, I. Y.; Kolesov, R.; Al-Hmoud, M.; Tisler, J.; Shin, C.; Kim, C.; Wojcik, A.; Hemmer, P. R.; Krueger, A.; Hanke, T.; Leitenstorfer, A.; Bratschitsch, R.; Jelezko, F. & Wrachtrup, J. (2008). Nanoscale imaging magnetometry with diamond spins under ambient conditions. *Nature*, Vol. 455, pp. 648-652

Balasubramanian, G.; Neumann, P.; Twitchen, D.; Markham, M.; Kolesov, R.; Mizuochi, N.; Isoya, J.; Achard, J.; Beck, J.; Tissler, J.; Jacques, V.; Hemmer, P. R.; Jelezko, F. & Wrachtrup, J. (2009). Ultralong spin coherence time in isotopically engineered diamond. *Nature Materials*, Vol. 8, pp. 383-387

Beveratos, A.; Brouri, R.; Gacoin, T.; Villing, A.; Poizat, J.-P. & Grangier, P. (2002). Single photon quantum cryptography. *Phys. Rev. Lett.*, Vol. 89, p. 187901

Craven, J. A.; Harte, B.; Fisher, D. & Schulze, D. J. (2009). Diffusion in diamond. I. Carbon isotope mapping of natural diamond. *Mineralogical magazine*, Vol. 73, pp. 193-200

Degen, C. L. (2008). Scanning magnetic field microscope with a diamond single-spin sensor. *Appl. Phys. Lett.*, Vol. 92, p.243111

Faklaris, O.; garrot, D.; Joshi, V.; Druon, F.; Boudou, J.-P., Sauvage, T.; Georges, P.; Curmi, P. A. & Treussart, F. (2008). Detection of single photoluminescent diamond nanoparticles in cells and study of the internalization pathway. *Small*, Vol. 4, pp. 2236-2239

Fu, C.-C.; Lee, H.-Y.; Chen, K.; Lim, T.-S.; Wu, H.-Y.; Lin, P.-K.; Wei, P.-K.; Tsao, P.-H.; Chang, H.-C. & Fann, W. (2007). Characterization and application of single fluorescent nanodiamonds as cellular biomarkers. *Proc. Natl. Acad. Sci. USA*, Vol. 104, pp. 727-732

Gruber, A.; Dräbenstedt, A.; Tietz, C.; Fleury, L.; Wrachtrup, J. & von Borczyskowski, C. (1997). Scanning confocal optical microscopy and magnetic resonance on single defect centres. *Science*, Vol. 276, pp. 2012-2015

Gurudev Dutt, M. V.; Childress, L.; Jiang, L.; Togan, E.; Maze, J.; Jelezko, F.; Zibrov, A. S.; Hemmer, P. R. & Lukin, M. D. (2007). Quantum register based on individual electronic and nuclear spin qubits in diamond. *Science*, Vol. 316, pp. 1312-1314

Hanbury Brown, R. & Twiss, R. Q. (1956). Correlation between photons in 2 coherent beams of light. *Nature*, Vol. 177, pp. 27-29

Harte, B.; Taniguchi, T. & Chakraborty, S. (2009). Diffusion in diamond. II. High-pressure-temperature experiments. *Mineralogical magazine*, Vol. 73, pp. 201-204

Hell, S. W. & Wichmann, J. (1994). Breaking the diffraction resolution limit by stimulated emission: stimulated-emission-depletion fluorescence microscopy. *Optics Letters*, Vol. 19, No.11, (June 1994), pp. 780-782

Hobler, G. (1996). Critical angles and low-energy limits to ion channeling in silicon. *Radiation effects and defects in solids*, Vol. 139, pp. 21-85

Jacques, V.; Wu, E.; Grosshans, F.; Treussart, F.; Grangier, P.; Aspect, A. & Roch, J.-F. (2007). Experimental realization of Wheeler delayed-choice gedanken experiment. *Science*, Vol. 315, pp. 966-968

Jelezko, F.; Gaebel, T.; Popa, I.; Gruber, A. & Wrachtrup, J. (2004). Observation of coherent oscillations in a single electron spin. *Phys. Rev. Lett.*, Vol. 92, p. 076401

Jelezko, F. & Wrachtrup, J. (2006). Single defect centres in diamond: a review. *Phys. Stat. Sol. (a)*, Vol. 203, pp. 3207-3225

Khan, H. A.; Khan, N. A. & Spohr, R. (1981). Scanning electron microscope analysis of etch pits obtained in a muscovite mica track detector by etching in hydrofluoric acid and aqueous solutions of NaOH and KOH. *Nucl. Instr. and Methods*, Vol. 189, pp. 577-581

Kurtsiefer, C.; Mayer, S.; Zarda, P. & Weinfurter, H. (2000). Stable solid-state source of single photons. *Phys. Rev. Lett.*, Vol. 85, pp. 290-293

Ladd, T. D.; Jelezko, F.; Laflamme, R.; Nakamura, Y.; Monroe, C. & O'Brien, J. L. (2010). Quantum computers. *Nature*, Vol. 464, pp. 45-53

Li, J.; Stein, D.; McMullan, C.; Branton, D.; Aziz, M. J. & Golovchenko J. A. (2001). Ion-beam sculpting at nanometre length scales. *Nature*, Vol. 412, pp. 166-169

Manson, N. B.; Harrison, J. P. & Sellars, M. J. (2006). Nitrogen-vacancy center in diamond : model of the electronic structure and associated dynamics. *Phys. Rev. B*, Vol. 74, p. 104303

Maze, J.; Stanwix, P. L.; Hodges, J. S.; Hong, S.; Taylor, J. M.; Cappelaro, P.; Jiang, L.; Gurudev Dutt, M. V.; Togan, E.; Zibrov, A. S.; Yacoby, A.; Walsworth, R. L. & Lukin, M. D. (2008). Nanoscale magnetic sensing with an individual electronic spin in diamond. *Nature*, Vol. 455, pp. 644-647

Meijer, J; Burchard, B.; Domhan, M.; Wittmann, C.; Gaebel, T.; Popa, I.; Jelezko, F. & Wrachtrup, J. (2005). Generation of single color centers by focused nitrogen implantation. *Appl. Phys. Lett.*, Vol.87, pp. 261909

Meijer, J.; Pezzagna, S.; Vogel, T.; Burchard, B.; Bukow, H. H.; Rangelow, I. W.; Sarov, Y.; Wiggers, H.; Plümel, I, Jelezko, F.; Wrachtrup, J.; Schmidt-Kaler, F.; Schnitzler, W.

& Singer, K. (2008). Towards the implanting of ions and positioning of nanoparticles with nm spatial resolution. *Appl. Phys. A*, Vol.91, pp. 567-571

Mohan, N.; Chen, C.-S.; Hsieh, H.-H.; Wu, Y.-C. & Chang, H.-C. (2010). In vivo imaging and toxicity assessments of fluorescent nanodiamonds in Caenorhabditis elegans. *Nano Letters*, Vol. 10, pp. 3692-3699

Naydenov, B.; Kolesov, R.; Batalov, A.; Meijer, J.; Pezzagna, S.; Rogalla, D.; Jelezko, F. & Wrachtrup, J. (2009). Engineering single photon emitters by ion implantation in diamond. *Appl. Phys. Lett.*, Vol. 95, p. 181109

Neumann, P.; Kolesov, R.; Naydenov, B.; Beck, J.; Rempp, F.; Steiner, M.; Jacques, V.; Balasubramanian, G.; Markham, M. L.; Twitchen, D. J.; Pezzagna, S.; Meijer, J.; Twamley, J.; Jelezko, F. & Wrachtrup, J. (2010). Quantum register based on coupled electron spins in a room-temperature solid. *Nature Physics*, Vol.6 , pp. 249-253

Persaud, A.; Ivanova, K.; Sarov, Y.; Ivanov, T.; Volland, B. E.; Rangelow, I. W.; Nikolov, N.; Schenkel, T.; Djakov, V.; Jenkins, D. W. K.; Meijer, J. & Vogel, T. (2006). Micromachined piezoresistive proximal probe with integrated bimorph actuator for aligned single ion implantation. *J. Vac. Sci. Technol. B*, Vol. 24, pp. 3148-3151

Pezzagna, S.; Naydenov, B.; Jelezko, F.; Wrachtrup, J. & Meijer, J. (2010). Creation efficiency of nitrogen-vacancy centres in diamond. *New J. Phys.*, Vol.12, pp. 065017

Pezzagna, S.; Wildanger, D.; Mazarov, P.; Wieck, A. D.; Sarov, Y.; Rangelow, I.; Naydenov, B.; Jelezko, F.; Hell, S. W. & Meijer, J. (2010). Nanoscale engineering and optical addressing of single spins in diamond. *Small*, Vol.6, pp. 2117-2121

Pezzagna, S.; Rogalla, D.; Wildanger, D.; Meijer, J. & Zaitsev, A. (2011). Creation and nature of optical centres in diamond for single-photon emission – overview and critical remarks. *New J. Phys.*, Vol.13, pp. 035024

Pezzagna, S.; Rogalla, D.; Becker, H.-W.; Jakobi, I.; Dolde, F.; Naydenov, B.; Wrachtrup, J.; Jelezko, F.; Trautmann, C. & Meijer, J. (2011). Creation of colour centres in diamond by collimated ion-implantation through nano-channels in mica. *Phys. Stat. Sol. (a)*, Vol. 208, pp. 2017-2022

Rittweger, E.; Han, K. Y.; Irvine S. E.; Eggeling, C & Hell, S. W. (2009). STED microscopy reveals colour centres with nanometric resolution. *Nature Photonics*, Vol.3, pp. 144-147

Schnitzler, W.; Linke, N. M.; Fickler, R.; Meijer, J.; Schmidt-Kaler, F. & Singer, K. (2009). Deterministic ultracold ion source targeting the Heisenberg limit. *Phys. Rev. Lett.*, Vol. 102, p. 070501

Spinicelli, P.; Dréau, A.; Rondin, L.; Silva, F.; Achard, J.; Xavier, S.; Bansropun, S.; Debuisschert, T.; Pezzagna, S.; Meijer, J.; Jacques, V. & Roch, J.-F. (2011). Engineered arrays of nitrogen-vacancy color centers in diamond based on implantation of CN- molecules through nanoapertures. *New J. Phys.*, Vol.13, pp. 025014

Taylor, J. M.; Cappellaro, P.; Childress, L.; Jiang, L.; Budker, D.; Hemmer, P. R.; Yacoby, A.; Walsworth, R. & Lukin, M. D. (2008). High-sensitivity diamond magnetometer with nanoscale resolution. *Nature Physics*, Vol. 4, p. 482

Toyli, D. M.; Weiss, C. D.; Fuchs, G. D.; Schenkel, T. & Awschalom, D. (2010). Chip-scale nanofabrication of single spins and spin arrays in diamond. *Nano Letters*, Vol.10, pp. 3168-3172
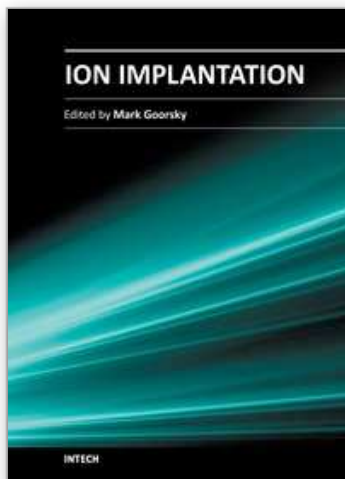
Zaitsev, A. M. (2001). Optical properties of diamond. A data handbook. (Springer) ISBN 3-540-66582-X

Ziegler, J. (2008). The stopping range of ions in matter, SRIM-2008, online at http://srim.org

Ion Implantation

Edited by Prof. Mark Goorsky

Ion implantation presents a continuously evolving technology. While the benefits of ion implantation are well recognized for many commercial endeavors, there have been recent developments in this field. Improvements in equipment, understanding of beam-solid interactions, applications to new materials, improved characterization techniques, and more recent developments to use implantation for nanostructure formation point to new directions for ion implantation and are presented in this book.

How to reference

In order to correctly reference this scholarly work, feel free to copy and paste the following:

INTECH
open science | open minds